AIAA AVIATION Forum
5-9 June 2017, Denver, Colorado
9th AIAA Atmospheric and Space Environments Conference

Check for updates

Numerical Study of an Iced Airfoil Based on Delayed Detached-Eddy Simulation with Low Dissipation Scheme

Maochao Xiao[1], Yufei Zhang*[2] and Haixin Chen[3]
School of Aerospace Engineering, Tsinghua University, Beijing, 100084, China

Unsteady and massive flow separation around a GLC-305 airfoil with a 22.5 min leading-edge horn ice accretion is numerically investigated using Delayed Detached-Eddy Simulation (DDES) based on shear layer stress transport model (SST). To resolve abundant turbulent structures, a low dissipation scheme called SLAU/MDCD is applied. The lift coefficient of the iced airfoil is well predicted by current approach with a relative error 1.2%, better than by 2D steady RANS, Dynamic Hybrid RANS/LES method (DHRL) and Zonal Detached Eddy Simulation method (ZDES). Although all methods underpredict the pressure plateau on the suction surface, DDES with low dissipation scheme reproduces the pressure plateau higher than the other methods, which shows better agreement with the experimental data. According to the time-averaged velocity field, the current DDES shows a reattachment position only slightly shorter instead of longer observed by other numerical studies than experimental result. Consequenly, low dissipation scheme is necessary to predict the separation bubble accurately. Finally, we conclude that DDES based on low disspation scheme is helpful to speed up the Kelvin-Helmholtz instability of free shear layer and capture abundant turbulent structures.

Downloaded by UNIVERSITY OF QUEENSLAND on June 8, 2017 | http://arc.aiaa.org | DOI: 10.2514/6.2017-3761

Nomenclature

a_1	=	parameter in SST turbulence model, $a_1 = 0.31$
C_{DES}	=	a parameter in DDES model
$C_{DES,k-\varepsilon}$	=	constant number, $C_{DES,k-\varepsilon} = 0.61$
$C_{DES,k-w}$	=	constant number, $C_{DES,k-w} = 0.78$
C_{d1}, C_{d2}	=	two constants in f_d function, $C_{d1} = 8, C_{d2} = 3$
C_μ	=	a parameter in SST turbulence model, $C_\mu = 0.09$
c	=	speed of sound
$\bar{c}$	=	sound speed average
c_k	=	weight in linear scheme
d_w	=	distance to the nearst wall
$\tilde{F}$	=	numerical flux
f_d	=	blending function in DDES
f_m	=	numerical dissipation function of in mass flux
f_p	=	numerical dissipation function of Ma in pressure
$h_{\max}$	=	maximum edge length of a cell
IS_k	=	smooth indicator in WENO scheme

[1] Graduate student, School of Aerospace Engineering, Tsinghua University, Student Member AIAA.
[2] Assistant professor, School of Aerospace Engineering, Tsinghua University, Senior Member AIAA. Corresponding author, email: zhangyufei@tsinghua.edu.cn
[3] Professor, School of Aerospace Engineering, Tsinghua University, Associate Fellow AIAA.
* Supported by National Key Basic Research Program of China (2014CB744801) and National Natural Science Foundation of China (11372160 and 11572177).

Copyright © 2017 by the American Institute of Aeronautics and Astronautics, Inc. All rights reserved.

k	=	turbulent kinetic energy of unit mass
LU-SGS	=	Lower-Upper Symmetric Gauss-Seidel Scheme
l_{DDES}	=	DDES length scale
l_{LES}	=	LES length scale
l_{RANS}	=	RANS length scale
MDCD	=	Minimized Dissipation and Controllable Dissipation Scheme
Ma	=	mach number
$\dot{m}$	=	mass flux rate
n_x, n_y, n_z	=	three components of face normal vector
P_k, P_w	=	production term in k equation
$\tilde{p}$	=	pressure flux
r	=	smooth indicator
SLAU	=	Parameter-Free Simple Low-Dissipation AUSM-Family Scheme
u, v, w	=	velocity components in x, y and z direction
u_j	=	velocity component in the j direction
V_n	=	velocity component normal to cell interface
w_k	=	weught in non-linear scheme
x_j	=	position vector in tensor notation
α	=	angle of attack
β	=	parameter in SST turbulence model
β^+, β^-	=	function of in AUSM-family schemes
γ_{disp}	=	free parameter in MDCD scheme controlling dispersion
γ_{diss}	=	free parameter in MDCD scheme controlling dissipation
ρ, e, p	=	density, total energy of unit mass, static pressure
σ	=	the weight of linear reconstruction to non-linear reconstruction
κ	=	karmen constant, $\kappa = 0.41$
μ, μ_t	=	molecular viscosity, eddy viscosity
σ_k, σ_w	=	parameters in SST turbulence model
ϕ	=	conservative variable
χ	=	a swithing function
Ω	=	vorticity magnitude, $\Omega = \sqrt{2\Omega_{ij}\Omega_{ij}}$
w	=	specific dissipation rate
Δ	=	right side value (-) minus left side value (+)
$+, -$	=	left and right side value at cell interface

Downloaded by UNIVERSITY OF QUEENSLAND on June 8, 2017 | http://arc.aiaa.org | DOI: 10.2514/6.2017-3761

I. Introduction

ICE accretion on a wing can severely degrade the aerodynamic performance of an aircraft. The flow field caused by an iced wing is characterized by a separation bubble downstream the ice horn, which results in decreased lift, increased drag, reduced stall angle of attack and loss of aircraft control effectiveness. Wind tunnel testing shows that even small ice accretions on the leading edge of an airfoil can result in a reduction in lift of 30% and an increase in drag of 40%[1]. The loss of lives attributed to ice accretion led the National Transportation Safety Board to marking icing as the most wanted aviation safety improvement[2].

Pan et al.[3] studied the effects of spanwise ice accretions on a modified NACA23012 airfoil with a simplified flap. Their investigation included steady-state simulations using RANS method based on solution-adaptive unstructured grid. The results showed that the pressure recovery cannot be accurately predicted and the discrepancy was attributed to the inability of steady RANS to capture the unsteady separation bubble downstream the ice horn. In general, steady RANS simulation underpredicts the maximum lift coefficient. Besides, the extent of separated flow was overpredicted even at low angle of attack. To simulate separated flow field more accurately, many researchers

has employed unsteady methods including Direct Numerical Simulation (DNS), Large Eddy Simulation (LES) and Detached Eddy Simulation (DES). Although the DNS resolves all spatial and temporal scales of turbulence, it is too expensive for high Reynolds flow. LES method was exploited by Brown[4] et al. to simulate large horn ice shape ICE4 configuration using purely tetrahedral mesh. Their results showed that lift coefficients predicted by LES were more accurate compared with RANS. Additionally, LES can capture rich inertial range vertical turbulence which is significant to improve lift prediction accuracy. While the required near-wall grid size by LES is comparable to DNS to simulate very small length and time scales of the near-wall turbulence. An attractive alternative to RANS and LES is DES[5][6]. This approach exploits the superiority of RANS method to simulate high Reynolds number attached boundary layer and the effectiveness of LES to solve unsteady three-dimensional separated flow. Pan et al.[7] performed a DES simulation for the NACA 23012 airfoil with forward-facing quarter-round simulated ice accretion. Their results showed that the maximum lift coefficient and stall angle predicted by DES were more consistent with experiments relative to RANS. Additionally, Choo[8], Lorenzo[9], Mogili[10] and Kumar[11] also reported improvement of the predicted results by DES-type approach.

Although original DES makes some success, it exhibits incorrect behavior in thick boundary layer and shallow separation regions[12][13][14]. This behavior begins when the grid spacing in parallel to the wall becomes less than boundary layer thickness whether due to grid refinement or boundary layer thickening. In these cases, the grid spacing is so small that LES branch activated inside the boundary layer, which is supposed to be RANS region. Early activation of LES branch inside the boundary layer can lead to the fact that resolved Reynolds stress deriving from velocity fluctuation is not enough to make up the reduction of modelled Reynolds stress. The depleted stress reduce the skin fraction, which further leads to premature separation. That is called Modelled Stress Depletion problem (MSD) or Grid Induced Separation problem (GIS). DDES proposed by Menter et al. in 2003[12][13] and Spalart et al. in 2006[14] solved the problem. In general, the switch between RANS and LES depends on not only grid spacing but also the specific flow features. Menter et al.[12][13] use the blending function in SST model to preserve RANS mode inside the boundary. Similarly, Spalart et al.[14] use a new parameter modified from S-A model to delay the transition from RANS mode to LES mode.

Alam et al.[1] and Lorenzo et al.[9] have explored the viability of DDES method in predicting lift and drag characteristics of an iced wing with horn ice shape near stall and streamwise ice shape post stall. Though showing some improvements in the calculation of lift and drag coefficients at high angle of attack, their simulation cannot accurately predict the huge detached zone and pressure distribution on the suction surface downstream of the ice. Alam et al.[1] points out that the DDES model shows a delayed shear layer instability aft the ice horn, which is the most common behavior occurs in the free shear layer caused by slow transition from RANS to LES. Thus, DDES overestimates the constant pressure and the length of pressure plateau aft the ice horn.

To accelerating the transition from RANS mode to LES mode, Zhang et al.[15] and Duclercq et al.[16] have applied Zonal Detached Eddy method (ZDES) to solve this issue. Unfortunately, Kelvin-Helmholtz instability is still retarded possibly due to the insufficient grid density, which increases the eddy viscosity in the shear layer. In contrast, Alam et al.[1] gain some success in capturing Kelvin-Helmholtz instability using DHRL model, whose RANS to LES transition is based on resolved turbulence production. While it should be noted that DHRL method predicts a slightly smaller separation bubble and its prediction to pressure distribution on the upper surface still shows a lot of offset from the experimental data.

This paper is to predict the separated flow around an iced airfoil based on DDES method with a low dissipation scheme, which is called SLAU/MDCD[17][18][19]. Also, it aims to improve the computation accuracy of pressure distribution and to study the effect of low dissipation scheme on accelerating the transition from RANS to LES.

II. Computational Methodology

A structured Navier-Stokes equation solver NSAWET (Navier-Stokes Analysis based on Window-Embedment Technology) was used in this study[19][20][21][22]. It is based on finite volume method with multi-block structured grid and is fully parallelized using the Message Passing Interface (MPI) library. The inviscid flux is calculated using SLAU/MDCD scheme[19]. The viscous term is discretized using second-order central difference scheme. For temporal discretization, time discretization is implemented using LU-SGS scheme with sub-iterations[23]. A brief description to SLAU/MDCD scheme and SST-DDES method will be presented in the following, more details can be found in references[14][17][18][19][24].

A. SLAU Scheme

Inviscid numerical flux is calculated by SLAU scheme, which is a new development of AUSM-family scheme. In contrast with existing all-speed schemes, SLAU features low-dissipation without any tunable parameters in low Mach number condition. At the same time, it keeps the robustness of the AUSM-family scheme against shock-

Downloaded by UNIVERSITY OF QUEENSLAND on June 8, 2017 | http://arc.aiaa.org | DOI: 10.2514/6.2017-3761

induced anomalies at high Mach number condition, such as carbuncle phenomenon and odd–even decoupling. To eliminate non-physical oscillation, mass flow is corrected in the scheme. The numerical flux of SLAU scheme is written as

$$\tilde{F}=\frac{\dot{m}+|\dot{m}|}{2}\Phi^{+}+\frac{\dot{m}-|\dot{m}|}{2}\Phi^{-}+\tilde{p}\vec{n}, \tag{1}$$

$$\Phi=(1,u,v,w,h)^{T}, \tag{2}$$

$$h=(e+p)/\rho, \tag{3}$$

$$\vec{n}=(0,n_x,n_y,n_z,0)^{T}. \tag{4}$$

Pressure flux $\tilde{p}$ is given by

$$\tilde{p}=\frac{p^{+}+p^{-}}{2}+\frac{\beta^{+}-\beta^{-}}{2}\left(p^{+}-p^{-}\right)+f_p\cdot\left(\beta^{+}+\beta^{-}-1\right)\frac{p^{+}+p^{-}}{2}, \tag{5}$$

where β^{+} and β^{-} are functions of *Ma* in AUSM-family schemes, f_p is introduced to decrease dissipation at low Mach number condition. In general, $f_p\propto|Ma|$ for $|Ma|<1.0$ and $f_p=1.0$ for $|Ma|\geq 1.0$. Mass flux is written as

$$\dot{m}=\frac{1}{2}\left\{(\rho V_n)^{+}+(\rho V_n)^{-}-|V_n|\Delta\rho\right\}f_m-\frac{\chi}{2\bar{c}}\Delta p, \tag{6}$$

where $f_m=1.0$ in weak expansion case and $f_m=1.0$ in supersonic strong expansion case. The added pressure term on the left right side is used to eliminate non-physical oscillation at low speed. and $\bar{c}$ is the average sound speed as $\bar{c}=\left(c^{+}+c^{-}\right)/2$. Detailed description to SLAU scheme can be found in reference[18].

B. MDCD Scheme

The interface states are reconstructed by fourth-order MDCD scheme. The scheme features minimized dispersion and controllable dissipation. Its dissipation can be adjusted to fit different cases without affecting minimized dispersion. Finite volume method based on MDCD reconstruction is capable of handling flow discontinuities and resolving a broad range of length scales. Thus, rich flow features encountered in practical engineering applications can be captured properly.

MDCD scheme is a weighted combination of the fourth-order linear and nonlinear scheme, its complete expression can be written as

$$\phi_{j+1/2}^{MDCD}=\sigma_{j+1/2}\phi_{j+1/2}^{linear}+\left(1-\sigma_{j+1/2}\right)\phi_{j+1/2}^{non-linear}. \tag{7}$$

The hybrid reconstruction reverts to linear reconstruction when $\sigma_{j+1/2}=1$ while to non-linear reconstruction when $\sigma_{j+1/2}=0$. $\sigma_{j+1/2}$ is determined by smooth indicator r_j.

$$\sigma_{j+1/2}=\min\left(1,r_{j+1/2}/r_c\right),\ r_{j+1/2}=\min\left(r_j,r_{j+1}\right), \tag{8}$$

$$r_j=\frac{\left|2\Delta\phi_{j+1/2}\Delta\phi_{j-1/2}\right|+\varepsilon}{\left(\Delta\phi_{j+1/2}\right)^2+\left(\Delta\phi_{j-1/2}\right)^2+\varepsilon}, \tag{9}$$

$$\Delta\phi_{j+1/2}=\phi_{j+1}-\phi_j. \tag{10}$$

In this paper, $r_c=0.4$ and $\varepsilon=5.6\times10^{-4}$. Depending on whether using linear weight c_k or non-linear weight w_k, the WENO scheme based on three-cell candidate stencils reads

$$\phi_{j+1/2}^{linear}=\sum_{k=0}^{3}c_k\phi_{j+1/2}^{k},\ \phi_{j+1/2}^{non-linear}=\sum_{k=0}^{3}w_k\phi_{j+1/2}^{k},\ k=0,1,2,3. \tag{11}$$

Here, c_k is optimized at the cost of reconstruction accuracy decreasing from sixth order to fourth order. It is determined by two free parameters γ_{disp} and γ_{diss} which control dispersion and dissipation separately. c_k can be expressed as

Downloaded by UNIVERSITY OF QUEENSLAND on June 8, 2017 | http://arc.aiaa.org | DOI: 10.2514/6.2017-3761

$$
\begin{aligned}
c_0 &= \frac{3}{2}\gamma_{disp} + \frac{3}{2}\gamma_{diss}, \\
c_1 &= \frac{1}{2} - \frac{3}{2}\gamma_{disp} + \frac{9}{2}\gamma_{diss}, \\
c_2 &= \frac{1}{2} - \frac{3}{2}\gamma_{disp} - \frac{9}{2}\gamma_{diss}, \\
c_3 &= \frac{3}{2}\gamma_{disp} - \frac{3}{2}\gamma_{diss}.
\end{aligned} \tag{12}
$$

The recommended values $\gamma_{disp} = 0.046$ and $\gamma_{diss} = 0.2$ are used in this paper. Then the non-linear weight c_k can be calculated similar to WENO scheme with $p_0 = 1$ as

$$
w_k = \left[\frac{c_k}{\varepsilon + IS_k}\right] \Big/ \sum_{k=0}^{3}\left[\frac{c_k}{\varepsilon + IS_k}\right],\ \varepsilon = 10^{-6}, \tag{13}
$$

where IS_k is the smooth indicator in WENO scheme. Details can be found in reference[17].

C. Turbulence Model

Travin et al.[25] and Zhang et al.[26] have compared the performance of SA-DES and SST-DES method. In the case of circular cylinder flow (Re=5.0E+04), two methods performs almost the same in terms of pressure distribution over the cylinder. The influence to prediction accuracy caused by the difference of background turbulence model is very little compared to the numerical scheme and grid quality[25]. Zhang et al.[26] applied the two methods to predict pressure distribution in the case of supersonic axisymmetric base flow. SST-DDES results fit better with experiment. Thus, SST-DDES is used in this paper. The governing equations of the SST-DDES model read as[14][24]

$$
\frac{\partial \rho k}{\partial t} + \frac{\partial \rho u_j k}{\partial x_j} = \frac{\partial}{\partial x_j}\left[\left(\mu + \sigma_k \mu_t\right)\frac{\partial k}{\partial x_j}\right] + P_k - C_\mu \frac{\rho k^{\frac{3}{2}}}{l_{DDES}}, \tag{14}
$$

$$
\frac{\partial \rho \omega}{\partial t} + \frac{\partial \rho u_j \omega}{\partial x_j} = \frac{\partial}{\partial x_j}\left[\left(\mu + \frac{\mu_t}{\sigma_\omega}\right)\frac{\partial \omega}{\partial x_j}\right] + 2\left(1 - F_1\right)\rho\sigma_{w2}\frac{1}{\omega}\frac{\partial k}{\partial x_j}\frac{\partial \omega}{\partial x_j} + P_\omega - \beta\rho\omega^2, \tag{15}
$$

$$
\mu_t = \min\left\{\frac{\rho k}{\omega}, \frac{\rho a_1 k}{\Omega F_2}\right\}, \tag{16}
$$

Here, F_1 and F_2 are SST blending functions[27]. P_k and P_ω are production terms in k-equation and ω-equation separately. The DDES length scale l_{DDES} reads as

$$
l_{DDES} = l_{RANS} - f_d \max\left(0, l_{RANS} - l_{LES}\right), \tag{17}
$$

$$
l_{LES} = C_{DES} h_{\max}, \tag{18}
$$

$$
l_{RANS} = \frac{\sqrt{k}}{C_\mu \omega}, \tag{19}
$$

$$
C_{DES} = F_1 \times C_{DES,k-\omega} + \left(1 - F_1\right) \times C_{DES,k-\varepsilon}. \tag{20}
$$

Here, $h_{\max}$ is the maximum edge length of the cell. The length scale l_{DDES} ranges between l_{RANS} and l_{LES}. The empirical blending function f_d is expressed as

$$
f_d = 1 - \tanh\left[\left(C_{d1} r_d\right)^{C_{d2}}\right], \tag{21}
$$

$$
r_d = \frac{\nu_T + \nu}{\kappa^2 d_w^2 \sqrt{\frac{\partial U_i}{\partial x_j}\frac{\partial U_i}{\partial x_j}}}. \tag{22}
$$

Here, d_w is the distance to the near wall. r_d is 1 in the LES region, thus $f_d = 0$ and $l_{DDES} = l_{LES}$; r_d is 0 in the RANS region, thus $f_d = 0$ and $l_{DDES} = l_{RANS}$. The parameter r_d is modified from its original definition in S-A model

Downloaded by UNIVERSITY OF QUEENSLAND on June 8, 2017 | http://arc.aiaa.org | DOI: 10.2514/6.2017-3761

in order to be more robust in irrotational region and be applied to other turbulent models[14]. Symbol meanings and constant values not given here can be found in the Nomenclature part or original references[12][14][24].

III. Geometry and Computational Grid

In this study, the GLC-305 airfoil with 944 ice shape was selected, which is a horn-type ice accretion produced by a 22.5 min exposure to glaze ice condition. Geometry and grid details are depicted as follows.

A. Geometry

The ice shape around the leading edge is illustrated in Figure 1. Height of the ice is around 0.05 chord length, which is the characteristic length referenced by meshing. The resulting flow features a high unsteady separated flow in the downstream of the ice. Experiments have been conducted in the Low-Turbulence Pressurized Tunnel (LTPT) by Addy et al.[29] and Broeren et al.[30]. Flow conditions in this study are Ma = 0.21, Re = 6.0E+06. The chord length and farfield freestream velocity are 0.9144m and 39.381m/s respectively. Experimental results show that the maximum lift coefficient was attained at about 6 deg. Thus numerical simulation at angle of attack 6 deg was conducted in this study. The simulation results including average aerodynamic force coefficient and average flow field are compared with experimental measurements[29][30].

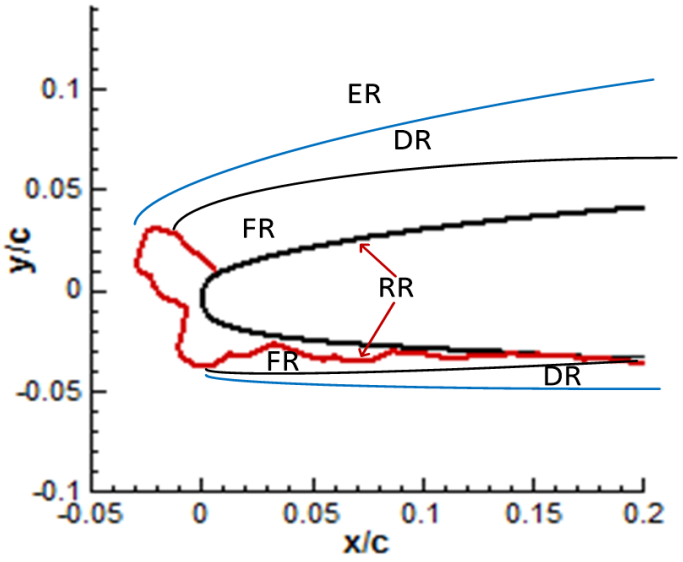

Figure 1. DDES zones for GLC-305 airfoil with 944 ice shape[32].
RR-RANS Region, FR-Focus Region, ER-Euler Region, DR-Departure Region between FR and ER.

B. Computational Grid

To remove any blockage effect caused by far-field boundaries, the computational domain boundaries were located approximately 50 chord length away from the iced airfoil. The spanwise length is 0.5 chord length. To decrease the number of grids, non-conformal patched grid was adopted in this study. Grid around and downstream of the ice shape on the upper surface is refined to capture small eddy structures. The height of the first grid point off the wall is 5E-06 chord length, so the dimensionless wall unit y^+ is less than 1.0 to ensure the accuracy of the near wall shear stress simulation. The growth rate in wall normal direction is 1.1. According the Spalart[31], a well-adjusted subgrid model should allow energy cascade to the smallest eddies that can be tracked on the mesh. Therefore, an eddy with a wavelength $\lambda = 5\Delta_0$ will be active even though it can not be highly accurate because it lacks the energy to smaller eddies[32]. Δ_0 is characteristic mesh spacing. In this study, an eddy with a wave length of less than 0.05c is intended to be resolved because the height of ice horn is 0.05c. Thus, mesh spacing in the focus region should be no more than 0.01c. focus region in this study has been illustrated in Figure 1. Separated turbulence in this region must be well resolved and mesh should be isentropic since the LES mode filters out eddies that are statistically isotropic. RANS region is primarily composed of boundary layer where there is no LES content. Detailed meshing requirements in different regions can be found in reference[31].

Downloaded by UNIVERSITY OF QUEENSLAND on June 8, 2017 | http://arc.aiaa.org | DOI: 10.2514/6.2017-3761

Figure 2(a) shows the non-conformal patched grid around the airfoil and Figure 2(b) shows the grid around the ice shape. In this study, DDES method have been implemented on three sets of mesh, which are coarse mesh, baseline mesh and refined mesh. The corresponding grid number are about 5 million, 15 million and 25 million.

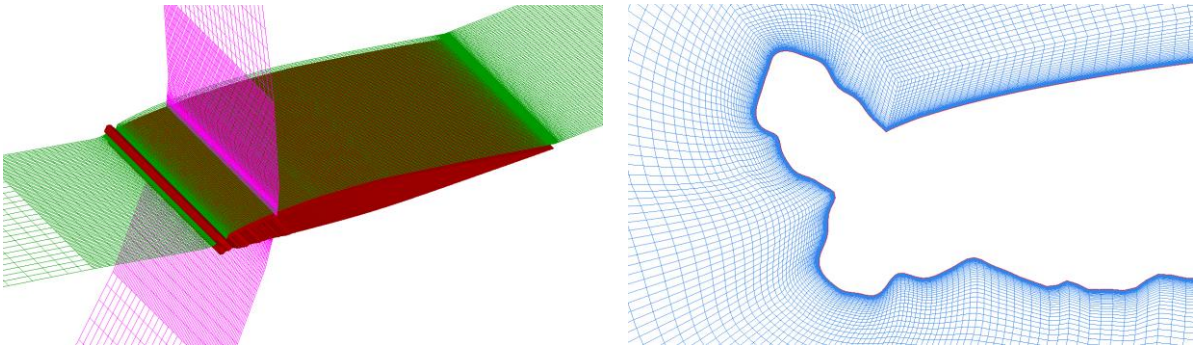

(a) **(b)**

Figure 2. Computational mesh. (a) Non-conformal patched grid around the airfoil (b) Grid around the ice shape

All calculations in this paper set no-slip and adiabatic wall boundary condition on the airfoil surface and non-reflecting boundary condition on the far-field boundary. A symmetry condition and a periodic condition were set on the spanwise boundaries for steady RANS simulation and unsteady DDES simulation respectively.

IV. Numerical Results

The time step is selected in such a way that the maximum Courant-Freidrichs-Lewy (CFL) number is approximately unity in the focus region based on the local maximum flow velocity $U_{\max}$, the local mesh size Δ_0 and the local time step. In this study, $U_{\max}$ is about 1.5 times of the free stream velocity. For coarse mesh, Δ_0 is about 0.004c and it yields a time step 0.060ms approximately. For baseline and refined mesh, Δ_0 is about 0.002c and 0.001c, which yields a time step 0.030ms and 0.015ms respectively. Non-dimensional time step are 0.0025, 0.0013 and 0.0006 based on the free stream velocity and the airfoil length.

The RANS simulations were carried out first to get steady solutions, whose results were then used as initial conditions for unsteady DDES simulations. The sudden decrease of eddy viscosity yields out a non-physical transient solution which must be removed. Therefore, physical solution results were collected and averaged after a non-dimensional time 50.

C. Comparison of Aerodynamic Force

The histories of the lift coefficients obtained from coarse mesh, baseline mesh and refined mesh, as well as the experimental results and 2D RANS results are plotted in Figure 3. It can be seen that mesh refinement has significantly improved the prediction of lift coefficients. In terms of lift coefficient, experiments yield the number 0.660 while simulation gives 0.467, 0.705, 0.695 and 0.668 for RANS, DDES on coarse, baseline and refined mesh respectively. The corresponding relative errors are -29.2%, 6.8%, 5.3% and 1.2%. The prediction to lift coefficient becomes more accurate by mesh refinement. In terms of drag coefficient, experiments yield the number 0.105 while simulations predict 0.086, 0.080, 0.106 and 0.084. The corresponding relative errors are -18.1%, -23.8%, -0.95% and -20.0%. The prediction of the drag coefficient are more challenging, which can also be found in references[1][15][32]. The main reason may be that experimental flow structures is more three-dimensional than DDES calculated flow, which might be caused by the spanwise variation of ice shape, as well as the finite span length of the model which induces possible corner flow at the side edge.

It should be noticed that the amplitude of force amplitude decreases with the mesh refined. This may be due to the fact that smaller turbulent structures can be resolved when the mesh scale decreases.

Downloaded by UNIVERSITY OF QUEENSLAND on June 8, 2017 | http://arc.aiaa.org | DOI: 10.2514/6.2017-3761

Downloaded by UNIVERSITY OF QUEENSLAND on June 8, 2017 | http://arc.aiaa.org | DOI: 10.2514/6.2017-3761

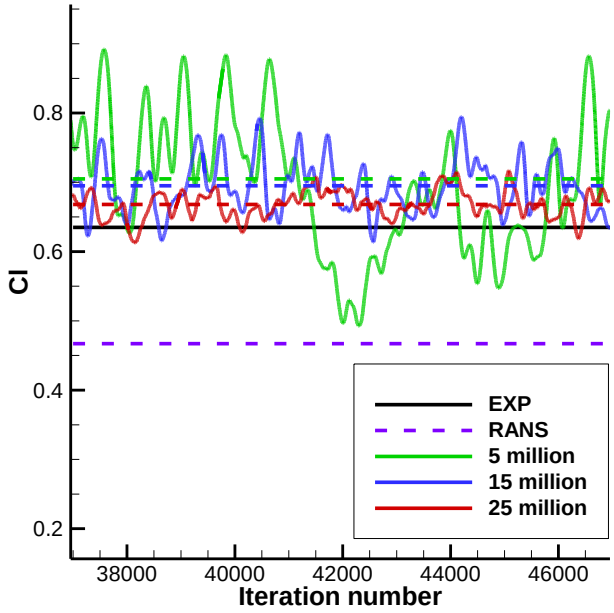

Figure 3. Histories of lift coefficient versus time steps for coarse mesh (green solid line), baseline mesh (blue solid line) and refined mesh (red solid line). Purple dashed line, green dashed line, blue dashed line and red dashed line are 2D RANS, DDES on coarse, baseline and refined mesh respectively. Black solid line is experimental result.

D. Time-averaged Surface Pressue Distribution

Figure 4 gives the comparison of calculated average surface pressure distribution by DDES on refined mesh with data from experiments[30] and references[1][15]. All calculations can predict the pressure in the region around the stagnation point correctly. Unfortunately, experiments by Broeren et al.[30] did not give the suction peak near the tip of the ice horn accurately, where the flow accelerates most. Thus we can not compare numerical prediction with experimental results at that point. Downstream of the suction peak, the pressure coefficient is characterized by a plateau with constant pressure resulting from large separation bubble. But this phenomenon is not observed in RANS calculation. In contrast, DDES can reproduce the pressure plateau in general though the current DDES method overestimates the constant pressure coefficient. Compared with results calculated by using DHRL[1] and ZDES[15], DDES can better predict the pressure plateau whether in term of its height or length. Because the suction peak predicted by DDES is much higher than DHLR model, its pressure plateau height is closer to the experiment. In the experiment, the constant pressure plateau extends to approximately 0.25c, while the DDES method predict a slightly longer plateau. Pressure distribution on the lower surface from all calculations including steady RANS shows good agreement with only small errors near the ice accretion, which may be due to inadequate grid resolution to the ice shape.

Downloaded by UNIVERSITY OF QUEENSLAND on June 8, 2017 | http://arc.aiaa.org | DOI: 10.2514/6.2017-3761

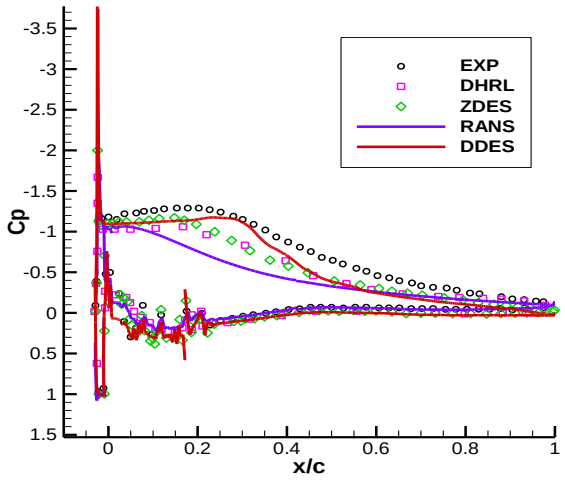

Figure 4. Comparison of mean surface pressure distribution by RANS and DDES with results from experiment[30], DHRL model[1] and ZDES model[15].

E. Time-averaged Velocity Field

Figure 5 demonstrates the time-averaged streamwise velocity around the iced airfoil. A large separation bubble is observed downstream of the horn ice. According to experiment, reattachment occurs at about 0.50c, while RANS calculation stretches the bubble length to 0.60c. Reattachment position predicted by DDES method is 0.46c, which is shorter and closer to the experiment. While all DDES results in reference[1][15] predict a much longer separation bubble. Thus, it is reasonable to expect that low numerical dissipation is necessary to predict the separation bubble accurately.

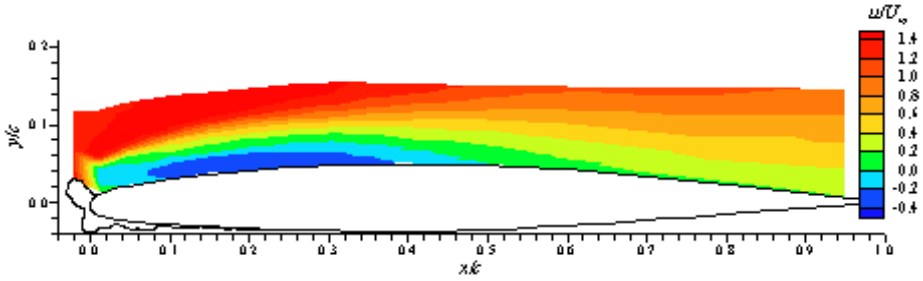

（a）PIV experiment result[30]

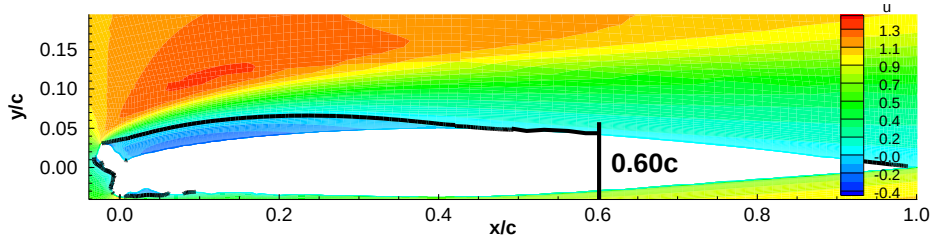

(b) RANS

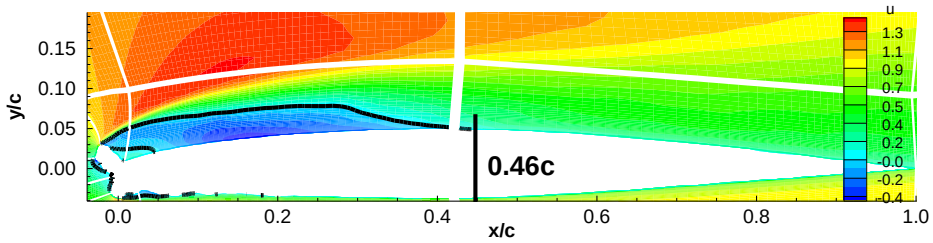

(c) DDES

Figure 5. Comparison of predicted midspan dimensionless time-averaged streamwise velocity by RANS and DDES with experimental data.

Downloaded by UNIVERSITY OF QUEENSLAND on June 8, 2017 | http://arc.aiaa.org | DOI: 10.2514/6.2017-3761

F. Instanteous Turbulent Structures

Figure 6 shows the instantaneous eddy structures colored by streamwise velocity at the non-dimensional time t=65 and t=75 by Roe/MUSCL scheme and SLAU/MDCD scheme. The eddy structures are depicted by Q criterion. The iso-surface qualitatively illustrates the complex unsteady separated flow. The flow features two dimension on the lower surface and ice shape but completely three dimension downstream of the horn ice. Turbulent flow separates at the horn tip, then the free mixing layer lose stability and rolls up into two dimensional spanwise vortex. Gradually, their two dimensional feature cannot be maintained and develops into completely three dimensional structures. Towards trailing edge, the turbulent structures become larger and more chaotic. Thus DDES with low dissipation is capable of resolving abundant and small turbulent vortex and simulating unsteady separated flow caused by ice accretion. By contrast, turbulent structures resolved by higher numerical dissipation scheme Roe/MUSCL are only large spanwise eddies. Small structures are dissipated numerically, which results in high frequency fluctuation parts in the turbulent kinetic energy spectra decreased. In addition, free shear layer predicted by Roe/MUSCL scheme is much longer the SLAU/MDCD scheme before losing insbility, which will be discussed further in the following.

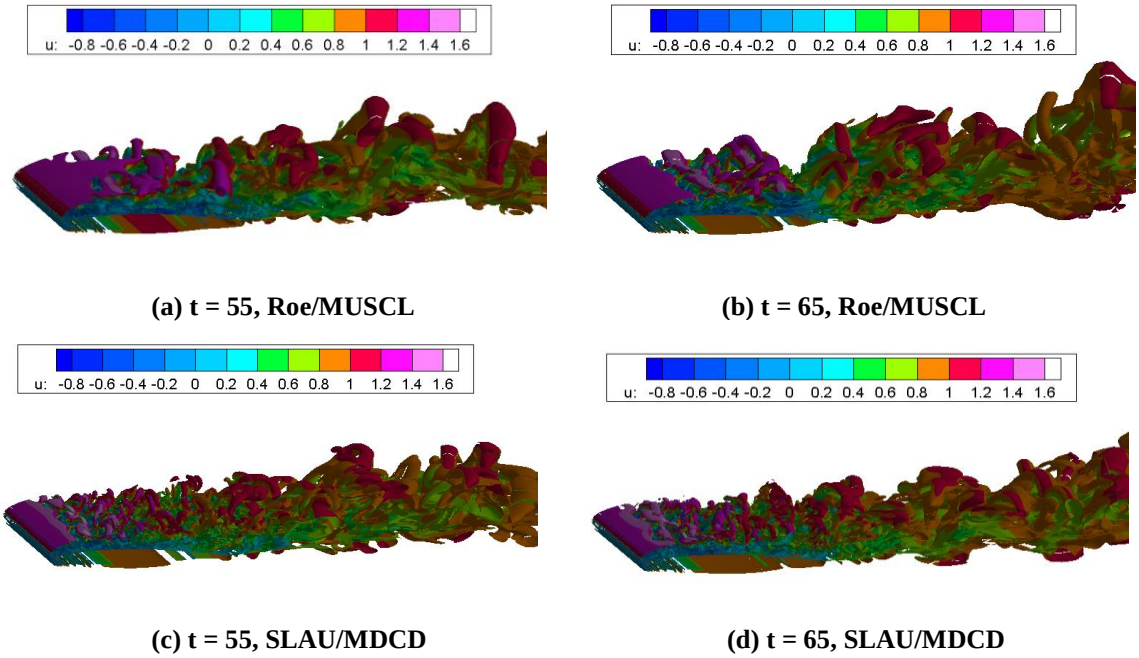

(a) t = 55, Roe/MUSCL

(b) t = 65, Roe/MUSCL

(c) t = 55, SLAU/MDCD

(d) t = 65, SLAU/MDCD

Figure 6. Instantaneous iso-surface of Q-criterion (Q = 0.1) at two dimensionless time t = 65 and t = 75.

G. Instanteous Vorticity Distribution

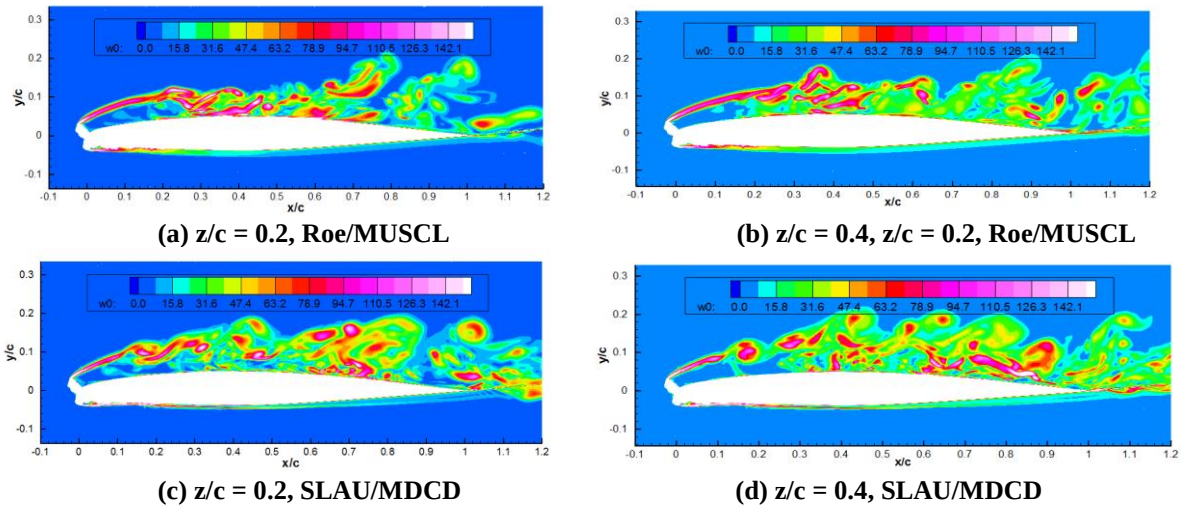

(a) z/c = 0.2, Roe/MUSCL **(b) z/c = 0.4, z/c = 0.2, Roe/MUSCL**

(c) z/c = 0.2, SLAU/MDCD **(d) z/c = 0.4, SLAU/MDCD**

Figure 7. Instantaneous vorticity distribution at two spanwise location z/c = 0.2 and z/c = 0.4 by Roe/MUSCL and SLAU/MDCD

Figure 7 shows the instantaneous distribution of vorticity magnitude at two spanwise location z = 0.2c and 0.4c calculated by DDES method using Roe/MUSCL scheme and SLAU/MDCD scheme. Due to the Kelvin-Helmholtz instability of free shear layer, strong vortexes shed from the tip of ice shape. Comparing vorticity distribution at the two spanwise locations calculated by SLAU/MDCD scheme, significant variations can be observed, which indicates a well-developed three dimensional turbulent flow. Although DDES results calculated by Roe/MUSCL scheme show spanwise variation in the vorticity structures, the three dimensional characteristic in the free mixing layer is much more conspicuous. DDES results in reference[1] based on bounded central difference scheme[33] and reference[9] based on Jameson's central scheme[34] also show the similar flow pattern. Thus, it is supposed to be that low numerical dissipation scheme is beneficial to speeding up the Kelvin-Helmholtz instability of free shear layer and capturing abundant turbulent structures.

Shur et al.[35] have put forward an enhanced version of DDES capable of accelerating transition from RANS to LES in separation flow through relating subscale length with not only the grid spacing but also kinematic, solution-dependent indicators of the 2D flow regions which allows a significant reduction of the subgrid viscosity in the initial region of the shear layer. Thus this new definition of subscale length is helpful to unlock the Kevin-Helmholtz instability and facilitate the development of realistic turbulent structures in the shear layers. Further work will be directed at the investigation of potential advantages using this new definition of subscale length with current low numerical dissipation scheme.

V. Conclusions

The SST-DDES method combined with low dissipation scheme SLAU/MDCD was applied in this study to improve prediction accuracy to massively separated flow around an iced airfoil at angle of attack around stall. The specific configuration is GLC-305 airfoil with 944 ice shape which is a glaze ice shape by a 22.5 min exposure to glaze ice condition. DDES results on three sets of mesh about 5 million, 15 million and 30 million have illustrated the grid convergence reasonably, with lift coefficients closer to experiment. Also, DDES results on refined mesh are compared with experimental data along with steady 2D RANS and other hybrid method including DHRL model[1] and ZDES model[15]. It has been shown that DDES method based on low dissipation scheme performs better in terms of the calculation of force coefficients, pressure distribution and recirculation zone:

(1) The relative error of lift coefficient is only 1.2%, which is far less than RANS and DHRL with -26.5% and -3.03%. The relative error of drag coefficient is -20.0%, which is similar to RANS and DhRL model.

(2) Though all methods overestimate the constant pressure coefficient of the pressure plateau on the suction surface, the DDES method exhibits better agreement with experimental data in terms of its height or length. Unfortunately, steady RANS fails to predict the pressure plateau. In addition, all simulations show similar results on the pressure surface.

(3) Reattachment position predicted by DDES calculation with low dissipation scheme is about 0.46c only slightly shorter instead of longer observed by others than experimental measurement. Thus, low numerical dissipation is helpful to improve the prediction accuracy to separation bubble.

Downloaded by UNIVERSITY OF QUEENSLAND on June 8, 2017 | http://arc.aiaa.org | DOI: 10.2514/6.2017-3761

(4) Low dissipation scheme is necessary for DDES method to speed up the transition from RANS to LES and unlock Kelvin-Helmholtz instability in free shear layer.

Based on the above analysis, we can conclude that SST-DDES method combined with low dissipation scheme is capable of resolving the development of small eddy structures and capturing the strong three dimensional unsteady effects. Still, more investigations are needed to improve prediction accuracy and better understand the separated flow features, which include:

(1) Investigating the impact of higher-order low dissipation schemes and adaptive dissipation schemes.

(2) Using the enhanced version of DDES proposed by Shur et al.[35] to accelerating the transition from RANS to LES in the initial region of mixing shear layer.

References

[1] Alam, M. F., Thompson, D. S., and Walters, D. K. "Hybrid Reynolds-Averaged Navier–Stokes/Large-Eddy Simulation Models for Flow Around an Iced Wing," *Journal of Aircraft*, Vol. 52, No. 1, 2015, pp. 1-13.

[2] Ratvasky, T. P., Barnhart, B. P., and Lee, S. "Current Methods Modeling and Simulating Icing Effects on Aircraft Performance, Stability, Control," *Journal of Aircraft*, Vol. 47, No. 1, 2010, pp. 201-211.

[3] Pan, J., and Loth, E. "Reynolds-Averaged Navier-Stokes Simulations of Airfoils and Wings with Ice Shapes," *Journal of Aircraft*, Vol. 41, No. 4, 2004, pp. 879-891.

[4] Brown, C. M., Kunz, R. F., Kinzel, M. P., Lindau, J., Palacios, J., and Brentner, K. S. "Large Eddy Simulation of Airfoil Ice Accretion Aerodynamics," *AIAA Atmospheric and Space Environments Conference*. 2013.

[5] Spalart, P. R., Jou, W.-H., Stretlets, M., and Allmaras, S. R. (1997), "Comments on the Feasibility of LES for Wings and on the Hybrid RANS/LES Approach", Advances in DNS/LES, *Proceedings of the First AFOSR International Conference on DNS/LES.*

[6] Strelets, M. "Detached eddy simulation of massively separated flows," *AIAA Fluid Dynamics Conference and Exhibit.* 2001.

[7] Pan, J., and Loth, E. "Detached Eddy Simulations for Airfoil with Ice Shapes," *AIAA Aerospace Sciences Meeting and Exhibit.* 2004.

[8] Choo, Y. K., Thompson, D., Mogili, P., Choo, Y. K., Thompson, D., and Mogili, P. "Detached-Eddy Simulations of Separated Flow Around Wings With Ice Accretions: Year One Report," 2004.

[9] Lorenzo, A., Valero, E., and Depablo, V. "DES/DDES Post-Stall Study with Iced Airfoil," *AIAA Aerospace Sciences Meeting Including the New Horizons Forum and Aerospace Exposition*. 2013.

[10] Mogili, P., Thompson, D., Choo, Y., and Addy, H. "RANS and DES Computations for a Wing with Ice Accretion." 2005.

[11] Kumar, S., and Loth, E. "Detached eddy simulations of an iced-airfoil," *Aerospace Sciences Meeting and Exhibit.* 2001.

[12] Menter, F. R., and Kuntz, M. Adaptation of Eddy-Viscosity Turbulence Models to Unsteady Separated Flow Behind Vehicles, 2004.

[13] Menter, F. R., Kuntz, M., and Langtry, R. "Ten years of industrial experience with the SST turbulence model. Turbulence," *Turbulence*, 2003.

[14] Spalart, P. R., Deck, S., Shur, M. L., Squires, K. D., Strelets, M. K., and Travin, A. "A New Version of Detached-eddy Simulation, Resistant to Ambiguous Grid Densities," *Theoretical and Computational Fluid Dynamics*, Vol. 20, No. 3, 2006, pp. 181-195.

[15] Zhang, Y., Habashi, W. G., and Khurram, R. A. "Zonal Detached-Eddy Simulation of Turbulent Unsteady Flow over Iced Airfoils," *Journal of Aircraft.* Vol. 53, No. 1, 2016, pp. 168-181.

[16] Duclercq, M., Brunet, V., and Moens, F. "Physical Analysis of the Separated Flow Around an Iced Airfoil Based on ZDES Simulations," 2012.

[17] Wang, Q., Ren, Y., Sun, Z., and Sun, Y. "Low dispersion finite volume scheme based on reconstruction with minimized dispersion and controllable dissipation," Science China Physics, *Mechanics and Astronomy*, Vol. 56, No. 2, 2013, pp. 423-431.

[18] Shima, E., and Kitamura, K. "Parameter-Free Simple Low-Dissipation AUSM-Family Scheme for All Speeds," *AIAA Journal*, Vol. 49, No. 8, 2011, pp. 1693-1709.

[19] Li, Z., Zhang, Y., and Chen, H. "A low dissipation numerical scheme for Implicit Large Eddy Simulation," *Computers & Fluids*, Vol. 117, 2015, pp. 233-246.

[20] Chen, H., S. Fu, and F.W. Li, "Navier-Stokes Simulations for Transport Aircraft Wing/Body High-Lift Configurations," *Journal of aircraft*, Vol. 40, No. 5, 2003, pp. 883-890.

[21] Chen, H., and Y. Zhang, et al., "Performance Prediction of Conical Nozzle using Navier-Stokes Computation," *49th AIAA/ASME/SAE/ASEE Joint Propulsion Conference*, 2013, San Jose, CA.

[22] Chen, H., and X. Huang, et al., "A Computational Fluid Dynamics Study of Circumferential Groove Casing Treatment in a Transonic Axial Compressor," *Journal of Turbomachinery*, Vol. 136, No. 3, 2014, pp. 031003.

[23] Jameson, A. "Time dependent calculations using multigrid, with applications to unsteady flows past airfoils and wings," 1991.

[24] Gritskevich, M. S., Garbaruk, A. V., Schütze, J., and Menter, F. R. "Development of DDES and IDDES Formulations for the k-ω Shear Stress Transport Model," Flow, *Turbulence and Combustion*, Vol. 88, No. 3, 2011, pp. 431-449.

Downloaded by UNIVERSITY OF QUEENSLAND on June 8, 2017 | http://arc.aiaa.org | DOI: 10.2514/6.2017-3761

[25] Travin, A., Shur, M., Strelets, M., and Spalart, P. R. "Physical and Numerical Upgrades in the Detached-Eddy Simulation of Complex Turbulent Flows," *Advances in Les of Complex Flows*, Vol. 65, 2002, pp. 239-254.
[26] Zhang, L .and Li. J.. Numerical simulations of supersonic base flow field based on RANS/LES approaches. *Acta Aeronautica et Astronautica Sinica*, Vol. 38, No. 1, 2017, pp. 120102-120102.
[27] Menter, F. R. "Two-equation eddy-viscosity turbulence models for engineering applications," *AIAA Journal*, Vol. 32, No. 8, 1994, pp. 1598-1605.
[28] Addy, and Harold, E. "Ice Accretions and Icing Effects for Modern Airfoils," Ice Accretions & Icing Effects for Modern Airfoils, 2000.
[29] Addy, H., Broeren, A., Zoeckler, J., and Lee, S. "A Wind Tunnel Study of Icing Effects on a Business Jet Airfoil," 2003.
[30] Broeren, A. P., Bragg, M. B., and Addy, H. E. "Flowfield Measurements About an Airfoil with Leading-Edge Ice Shapes," *Journal of Aircraft*, Vol. 43, No. 4, 2015, pp. 1226-1234.
[31] Philippe R., S. Young-Person"s Guide to Detached-Eddy Simulation Grids: NASA Langley Technical Report Server, 2001.
[32] Choo, Y. K., Thompson, D., Mogili, P., Choo, Y. K., Thompson, D., and Mogili, P. "Detached-Eddy Simulations of Separated Flow Around Wings With Ice Accretions: Year One Report," 2004.
[33] Jasak, H., Weller, H.G., Gosman, A. D. High resolution NVD differencing scheme for arbitrarily unstructured meshes[J]. *International Journal for Numerical Methods in Fluids*, Vol. 31, No. 2, 1998, pp. 709-737.
[34] Jameson, A., Schmidt, W., Turkel, E. Numerical solution of the Euler equations by finite volume methods using Runge Kutta time stepping schemes[J]. 1981, 1259(11):2004--4325.
[35] Shur, M. L., Spalart, P. R., Strelets, M. K., and Travin, A. K. "An Enhanced Version of DES with Rapid Transition from RANS to LES in Separated Flows," Flow, Turbulence and Combustion, Vol. 95, No. 4, 2015, pp. 709-737.

Downloaded by UNIVERSITY OF QUEENSLAND on June 8, 2017 | http://arc.aiaa.org | DOI: 10.2514/6.2017-3761